2011 IEEE International Conference on Control Applications (CCA)
Part of 2011 IEEE Multi-Conference on Systems and Control
Denver, CO, USA. September 28-30, 2011

Model-based analysis and control of axial and torsional stick-slip oscillations in drilling systems

Bart Besselink, Nathan van de Wouw, Henk Nijmeijer

Abstract— **The mechanisms leading to torsional vibrations in drilling systems are considered in this paper. Thereto, a drill string model of the axial and torsional dynamics is proposed, where coupling is provided by a rate-independent bit-rock interaction law. Analysis of this model shows that the fast axial dynamics exhibit an axial stick-slip limit cycle. This generates an apparent velocity-weakening effect in the torque-on-bit, explaining the onset of torsional vibrations. Based on this analysis, a strategy for control design aiming at the suppression of torsional vibrations is presented.**

I. Introduction

Rotary drilling systems using drag bits, as used for the exploration and production of oil and gas, are known to exhibit torsional vibrations, which may lead to torsional stick-slip. These stick-slip oscillations decrease drilling efficiency, accelerate the wear of drag bits and may cause drill string failure because of fatigue. The mechanisms leading to these torsional vibrations are analyzed in this work. Additionally, this analysis facilitates the development of a control strategy targeting the stabilization of the torsional dynamics.

In the analysis of torsional vibrations, most studies use models that account for the torsional dynamics only. Generally, the resisting torque-on-bit as a result of bit-rock interaction is trivialized by modeling it as a frictional contact with a (locally) velocity-weakening effect (see e.g. [1], [2], [3]). In these models, the rate effect is thus considered as an intrinsic property of the processes taking place at the bit-rock interface. However, experiments using single cutters, aiming at the identification of the bit-rock interaction law, have not revealed any velocity-weakening effect [4].

This discrepancy led to a different approach, initiated in [5], where both the axial and torsional dynamics of a drill string are modeled. These dynamics are coupled using a rate-independent bit-rock interaction law developed in [6], which generates a regenerative effect. Analysis of this model in [5], [7] shows that the axial dynamics exhibit a stick-slip limit cycle. This axial limit cycle generates an apparent velocity-weakening effect in the torsional dynamics, leading to torsional vibrations. Herein, the rate effect is the result of the interaction between axial and torsional dynamics, rather than an intrinsic property of the bit-rock interaction law.

The model as analyzed in [7] lacks the essential aspects of axial flexibility of the drill string and dissipation due to friction along the bottom hole assembly in axial direction. In the current work, as in [8], axial stiffness and damping are included and a more realistic model is obtained. In addition, the torsional dynamics of the rotary table is included in the current paper. This does not only lead to a more realistic model, it also allows for the design of controllers for the torsional dynamics, where the torque on the rotary table is employed as the control input.

Following [7] and [8], the *onset* of torsional vibrations is analyzed by averaging the influence of the fast axial dynamics on the slow torsional dynamics. Here, it is shown that the axial dynamics exhibit a stick-slip limit cycle, which generates an apparent velocity-weakening effect in the torque-on-bit. This rate effect is responsible for the onset of torsional vibrations. The analysis of these phenomena is beneficial from two perspectives. First, it supports the development of improved drill-string and bit design less prone to stick-slip vibrations. Second, it facilitates the design of controllers aiming to mitigate torsional vibrations. In the current paper, a controller is designed based on the torsional dynamics only, where the apparent velocity-weakening effect due to the axial vibrations is taken into account. Thus, this approach differs from other strategies to suppress the torsional vibrations (see e.g. [9], [10], [11], [12]), where models are used in which the bit-rock interaction is trivialized as a frictional contact.

Besides the design of controllers targeting the torsional vibrations directly, the analysis discussed in the current paper might facilitate novel control strategies aiming at the stabilization of the axial dynamics. Since the onset of torsional vibrations is due to an apparent velocity-weakening effect generated by the axial dynamics, the controlled stabilization of the axial dynamics may also prevent torsional vibrations.

The outline of this paper is as follows. First, the drill string model is introduced in Section II. Then, the axial dynamics is analyzed in Section III, resulting in an averaged representation that is exploited in the analysis of the torsional dynamics in Section IV. Then, the design of a controller for the stabilization of the torsional dynamics is discussed in Section V. Finally, conclusions are presented in Section VI.

II. Modeling

The drilling system model as depicted in Fig. 1 is considered. Here, the bottom mass, with mass M and inertia I_1, represents the bottom hole assembly (BHA), whose axial and angular position are denoted by $U(t)$ and $\Phi(t)$, respectively. The bottom hole assembly is connected to the rotary table by a drill pipe, which is modeled as a spring with axial stiffness K and torsional stiffness C. The rotary table, with angular position $\Theta(t)$, is modeled by an inertia I_2, to which a torque

Bart Besselink, Nathan van de Wouw and Henk Nijmeijer are with the Dynamics and Control group, Department of Mechanical Engineering, Eindhoven University of Technology, P.O. Box 513, 5600 MB Eindhoven, the Netherlands, b.besselink@tue.nl, n.v.d.wouw@tue.nl, h.nijmeijer@tue.nl

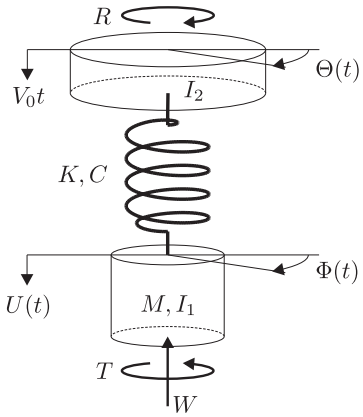

Fig. 1. Drill string model.

R is applied to drive the drilling system. Additionally, it is assumed that the axial position of the top of the drill string is prescribed as V_0t, which represents the position of the hook. This leads to the following equations of motion

$$M\frac{d^2U}{dt^2} + D\frac{dU}{dt} + K(U - V_0t) = -W^c - W^f, \quad (1)$$

$$I_1\frac{d^2\Phi}{dt^2} + C(\Phi - \Theta) = -T^c - T^f, \quad (2)$$

$$I_2\frac{d^2\Theta}{dt^2} + C(\Theta - \Phi) = R. \quad (3)$$

Here, W^i and T^i ($i \in \{c, f\}$) denote the axial force and torque on the drill bit as a result of the bit-rock interaction, respectively. Following [6], the forces are assumed to be the result of two different processes. First, the removal of rock is described by a cutting process, which is modeled as

$$W^c = na\zeta\varepsilon d, \qquad T^c = \tfrac{1}{2}na^2\varepsilon d, \quad (4)$$

with n the number of blades and a the radius of the drill bit. The intrinsic specific energy ε represents the required energy to destroy a unit volume of rock, whereas ζ characterizes the orientation of the cutting face. Furthermore, the cutting forces are proportional to the depth-of-cut d, which is in general not constant. Specifically, the depth-of-cut is dependent on the current axial position of the bottom hole assembly and the profile of the well bottom, as generated by the previous blade some time t_n earlier. This leads to

$$d(t) = U(t) - U(t - t_n(t)), \quad (5)$$

where the delay t_n represents the time interval in which the bit rotates $2\pi/n$ rad, which is the angle between two successive blades. Thus, t_n is described implicitly as

$$\Phi(t) - \Phi(t - t_n(t)) = \frac{2\pi}{n}. \quad (6)$$

The second process is the result of the interaction between the underside of the blades, known as the wearflat, and the well bottom. This contact is described by the contact stress $\bar{\sigma}$, which is independent of the drilling velocity. However, the geometry of the bit-rock contact shows that the wearflat is no longer in contact with the well bottom when the bit moves upwards. Then, the contact forces are modeled as

$$W^f = \frac{nal\bar{\sigma}}{2}\left(1 + \mathrm{sign}\left(\frac{dU}{dt}\right)\right), \quad T^f = \tfrac{1}{2}a\xi\mu W^f, \quad (7)$$

where the sign function describes whether or not the wearflat, with length l, is in contact with the well bottom. A frictional process relates the axial contact force to the friction torque via the friction coefficient μ and the parameter ξ, which characterizes the spatial distribution of the wearflats.

Since drill string vibrations are of interest, perturbations from the nominal solutions of (1-3) are considered. For a given nominal torque R_0 and axial velocity V_0, the solutions of (1-3) in the absence of vibrations are denoted by $U_0(t)$, $\Phi_0(t)$ and $\Theta_0(t)$, respectively. These solutions correspond to a constant rotational speed Ω_0, leading to a constant delay t_{n0} and depth-of-cut d_0 satisfying

$$d_0 = \frac{R_0 - \frac{1}{2}na^2\xi\mu l\bar{\sigma}}{\frac{1}{2}na^2\varepsilon} = \frac{2\pi}{n}\frac{V_0}{\Omega_0} = V_0t_{n0}. \quad (8)$$

To reduce the number of parameters, the equations of motion are scaled using the characteristic time $t_* = \sqrt{I_1/C}$ and length $L_* = 2C/\varepsilon a^2$. Here, $2\pi t_*$ is the period time related to the torsional resonance frequency; L_* represents the total penetration per revolution for a sharp cutter ($l = 0$) inducing a one radian twist in the drill string. Typically, $t_* \sim 1$s and $L_* \sim 1$mm. Then, scaled relative coordinates are defined as

$$u(\tau) = \frac{U(t) - U_0(t)}{L_*}, \quad (9)$$

$$\varphi(\tau) = \Phi(t) - \Phi_0(t), \quad \theta(\tau) = \Theta(t) - \Theta_0(t) \quad (10)$$

with $\tau = t/t_*$ the scaled time. Additionally, $u(\tau)$, $\varphi(\tau)$ and $\theta(\tau)$ represent the (scaled) relative axial and angular positions, whose dynamics is described by

$$\ddot{u}(\tau) + \gamma\dot{u}(\tau) + \eta^2u(\tau) = n\psi\big[-v_0(\tau_n - \tau_{n0}) - u(\tau) + u(\tau - \tau_n) + \lambda g(\dot{u}(\tau))\big], \quad (11)$$

$$\ddot{\varphi}(\tau) + (\varphi(\tau) - \theta(\tau)) = n\big[-v_0(\tau_n - \tau_{n0}) - u(\tau) + u(\tau - \tau_n) + \beta\lambda g(\dot{u}(\tau))\big], \quad (12)$$

$$\rho\ddot{\theta}(\tau) + (\theta(\tau) - \varphi(\tau)) = \mathcal{R} - \mathcal{R}_0. \quad (13)$$

Here, (4), (7) and (5) are used. In these coordinates, the delay $\tau_n = t_n/t_*$ is described by

$$\varphi(\tau) - \varphi(\tau - \tau_n) + \omega_0\tau_n = 2\pi/n, \quad (14)$$

with ω_0 the nominal angular velocity in the dimensionless time scale, i.e. $\omega_0 = \Omega_0t_*$. Similarly, v_0 (in (11-12)) is the scaled nominal axial velocity $v_0 = V_0t_*/L_*$. In (11), γ and η denote the scaled axial damping and stiffness parameters; ψ characterizes the drill string design:

$$\gamma = \frac{D}{M}\sqrt{\frac{I_1}{C}}, \quad \eta = \sqrt{\frac{KI_1}{MC}}, \quad \psi = \frac{\zeta\varepsilon aI_1}{MC}. \quad (15)$$

The influence of the contact forces is given by λ, which is a measure for the bluntness of the drill bit. Therefore, it equals zero for a perfectly sharp cutter. In (12), the parameter β is dependent on the drill bit design. Finally, in (13), ρ denotes

the ratio of the inertias, whereas $\mathcal{R} - \mathcal{R}_0$ denotes the scaled deviation from the nominal torque, such that

$$\lambda = \frac{a^2 l \bar{\sigma}}{2\zeta C}, \quad \beta = \zeta\mu\xi, \quad \rho = \frac{I_2}{I_1}, \quad \mathcal{R} = \frac{R}{C}, \quad \mathcal{R}_0 = \frac{R_0}{C}. \tag{16}$$

Because of scaling, all parameters are of $\mathcal{O}(1)$. Typically, the only exception is ψ in (15), which, for a large class of drilling systems, is of order $\mathcal{O}(10^2 - 10^3)$.

The contact forces are represented in (11) and (12) by the nonlinear function $g(\dot{u}(\tau))$, which indicates whether the wearflat is in contact with the well bottom ($g = 0$) or not ($g = 1$). The discontinuity at $dU/dt = 0$ ($\dot{u} = -v_0$) in (7) is replaced by a convex set-valued map, hereby adopting Filippov's solution concept [13]:

$$g(\dot{u}(\tau)) \in \frac{1 - \mathrm{Sign}(v_0 + \dot{u}(\tau))}{2} = \begin{cases} 0, & \dot{u} > -v_0, \\ [0,1], & \dot{u} = -v_0, \\ 1, & \dot{u} < -v_0. \end{cases} \tag{17}$$

Here, Sign denotes the set-valued sign function. Then, the total model describing the dynamics of the perturbation from the nominal trajectory is given by (11-14) and the set-valued map (17), which constitutes a delay-differential inclusion.

The model (11-14) with (17) describes the dynamics of a drill string for nonnegative depth-of-cut ($d \geq 0$) and positive angular speed of the drill bit ($\dot{\varphi} > -\omega_0$). Thus, the model loses validity when the depth-of-cut becomes negative, indicating that the bit is no longer in contact with the well bottom. This can be caused by severe axial vibrations and is known as bit bouncing. Since bit bouncing causes damage to the drill bit, it should be avoided at all times and is not considered in this work. In addition, torsional stick is not included in the model (11-14). Nonetheless, the model can be used to predict the *onset* of torsional vibrations (which can lead to stick-slip). An approach for the inclusion of torsional stick in the model (11-14) is given in [8].

III. Axial dynamics

For a broad class of drilling systems, two distinct time scales can be identified due to the magnitude of the parameter ψ, which is typically of order $\mathcal{O}(10^2 - 10^3)$. Namely, the axial dynamics (11) is fast when compared to the torsional dynamics (12-13), which allows for the individual analysis of the axial dynamics (see also [7]). In this analysis, the slowly varying angular velocity can be considered constant. To emphasize this fast time scale, the time $\bar{\tau} = \tau\sqrt{n\psi}$ is introduced, such that (11) can be written as

$$\bar{u}''(\bar{\tau}) + \bar{\gamma}\bar{u}'(\bar{\tau}) + \bar{\eta}^2\bar{u}(\bar{\tau}) = -\bar{u}(\bar{\tau}) + \bar{u}(\bar{\tau} - \bar{\tau}_n) + \frac{\lambda}{\bar{v}_0}\bar{g}(\bar{u}'(\bar{\tau})), \tag{18}$$

where the scaled coordinate $\bar{u}$ is defined as

$$\bar{u}(\bar{\tau}) = \frac{u(\tau)}{\bar{v}_0} + \frac{\bar{\tau}_n - \bar{\tau}_{n0}}{\bar{\eta}^2} \tag{19}$$

and $'$ denotes differentiation with respect to the fast time $\bar{\tau}$. In addition, $\bar{\tau}_n = \tau_n\sqrt{n\psi}$ and $\bar{\tau}_{n0} = \tau_{n0}\sqrt{n\psi}$. In (19), the delay $\bar{\tau}_n$ is constant, which results from the assumption that the slowly varying angular velocity is constant. In the fast axial dynamics (18), the nonlinearity $\bar{g}(\bar{u}'(\bar{\tau}))$ is given by

$$\bar{g}(\bar{u}'(\bar{\tau})) \in \frac{1 - \mathrm{Sign}(1 + \bar{u}'(\bar{\tau}))}{2}, \tag{20}$$

whereas the parameters are scaled as $\bar{\gamma} = \gamma/\sqrt{n\psi}$, $\bar{\eta} = \eta/\sqrt{n\psi}$ and $\bar{v}_0 = v_0/\sqrt{n\psi}$.

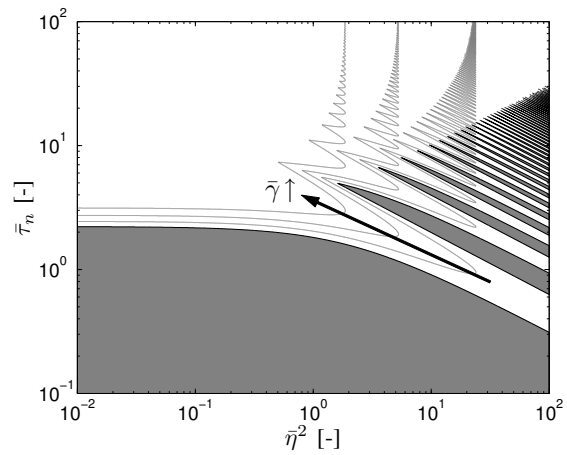

Fig. 2. Stability diagram for the axial dynamics for $\bar{\gamma} \in \{0, 0.2, 0.4, 0.6\}$. The gray and white region denote the stable and unstable region, respectively, for $\bar{\gamma} = 0$. The lines denote the stability boundary for increasing damping parameter $\bar{\gamma}$.

In (18), the equilibrium $\bar{u} = 0$ corresponds to a constant axial velocity. Since the delay τ_n is assumed to be constant, this implies a constant depth-of-cut. Around this equilibrium point, the full contact force is active (i.e. $\bar{g}(\bar{u}'(\bar{\tau})) = 0$), such that local stability properties can be investigated by considering the characteristic equation

$$P(s) = s^2 + \bar{\gamma}s + \bar{\eta}^2 + 1 - e^{-s\bar{\tau}_n} = 0. \tag{21}$$

The roots of (21) are determined by the method of τ-decomposition [14]. The result of this analysis is depicted in Fig. 2, which shows the stability boundary in the parameter space. Here, it can be seen that a single stability boundary is obtained for small stiffness parameter $\bar{\eta}^2$. On the other hand, multiple stability regions emerge for high $\bar{\eta}^2$, caused by the complex interaction between the dynamics and the delay. Also, it can be concluded that an increase in the damping parameter $\bar{\gamma}$ increases the region in which stability can be guaranteed. However, for realistic values of the delay $\bar{\tau}_n$ (of $\mathcal{O}(10 - 10^2)$) and the parameters $\bar{\eta}^2$ and $\bar{\gamma}$ (both of $\mathcal{O}(0.1)$), the axial equilibrium point is unstable.

For these realistic parameter values, small perturbations around the axial equilibrium point grow, resulting in an axial limit cycle. A typical example of this axial stick-slip limit cycle is depicted in Fig. 3, where the slip and stick phases can clearly be observed. In the slip phase of the axial limit cycle, the bit moves downward and the full contact force is mobilized, i.e. $\bar{g} = 0$. When the axial velocity reaches zero (i.e. $\bar{u}' = -1$ in Fig. 3), the discontinuity in these contact forces causes the bit to stick. Physically, the contact forces W^f can compensate for the cutting forces W^c and the forces exerted by the drill string, maintaining the stick phase. Nonetheless, due to the positive rotational speed, the bit still

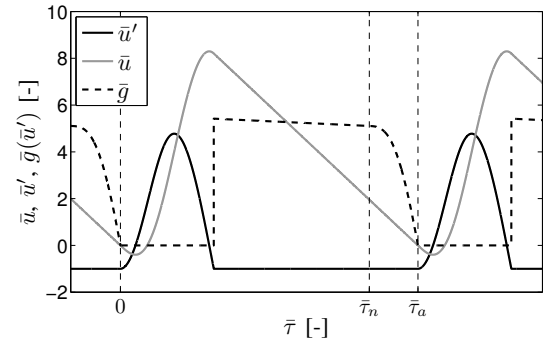

Fig. 3. Axial limit cycle example in scaled coordinate $\bar{u}(\bar{\tau})$.

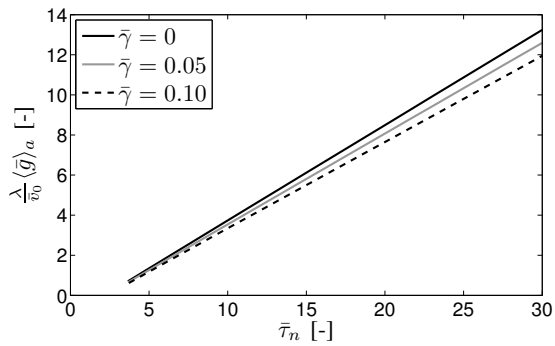

Fig. 4. Averaged value of the nonlinearity $\frac{\lambda}{\bar{v}_0}\bar{g}(\bar{u}'(\bar{\tau}))$ over one axial limit cycle, for $\bar{\eta}^2 = 0.1$ and varying $\bar{\gamma}$.

removes rock. Even though the bit sticks axially and does not move downward, the depth-of-cut (to which the cutting forces W^c are proportional) is not necessarily constant, as the rock profile generated by the previous blade may change. At $\bar{\tau} > \bar{\tau}_n$, the cutting forces W^c increase, leading to an increase in the contact forces W^f to maintain the stick phase. This can be observed as the decrease of the nonlinearity $\bar{g}$ in Fig. 3. When the contact forces cannot be increased any further ($\bar{g} = 0$), the bit starts to move axially again, entering a new slip phase. More details on the axial stick-slip limit cycle can be found in [8], where a semi-analytical approach for the computation of the limit cycles is proposed.

In the absence of axial vibrations, the full contact stress is mobilized and $\bar{g} = 0$. Clearly, this does not hold for the axial stick-slip limit cycle in Fig. 3. Instead, the contact forces W^f decrease (i.e. $\bar{g} > 0$) in the stick phase, such that the presence of axial vibrations causes the averaged contact forces to decrease. This effect is quantified by considering the average value of the nonlinearity (20) over one axial limit cycle given as $\langle\bar{g}\rangle_a := \int_0^{\bar{\tau}_a} \bar{g}(\bar{u}'(\bar{\tau}))\,\mathrm{d}\bar{\tau}$, where $\bar{\tau}_a$ is the period time of the axial limit cycle. Since the axial stick-slip limit cycle is dependent on the delay $\bar{\tau}_n$, the value of $\langle\bar{g}\rangle_a$ is a function of $\bar{\tau}_n$ as well, as depicted in Fig. 4 for some parameter values. Here, it is noted that the value of $\bar{g}$ in the stick phase is such that stick is maintained (i.e. $\bar{u}' = \bar{u}'' = 0$ in the dynamics (18)), prescribing the value of $\frac{\lambda}{\bar{v}_0}\bar{g}$. Stated differently, the average value of $\frac{\lambda}{\bar{v}_0}\bar{g}$ is dependent on the axial limit cycle, which in turn only depends on the delay and the stiffness and damping parameters. From Fig. 4 it can be observed that the averaged contact forces are a linear function of the delay $\bar{\tau}_n$, where the slope is dependent on the parameters $\bar{\gamma}$, $\bar{\eta}$. However, the dependence of $\bar{\eta}$ is minor and is not shown here. The computation of $\langle\bar{g}\rangle_a$ relies on the semi-analytical approach of the axial limit cycles in [8], which does not apply to small values of τ_n (see [8] for details). However, when linear approximations are extrapolated for small delay, it is found that the point $\langle\bar{g}\rangle_a = 0$ is obtained for $\bar{\tau}_n = \bar{\tau}_n^{crit}$, where $\bar{\tau}_n^{crit}$ is the critical delay at which stability of the axial equilibrium point is lost. Hence, $\bar{\tau}_n^{crit}$ is on the stability boundary in Fig. 2 and the axial limit cycle only exists for $\bar{\tau}_n > \bar{\tau}_n^{crit}$. Then, an approximation of the averaged contact forces is given as

$$\langle\bar{g}\rangle_a \approx \frac{\bar{v}_0}{\lambda} A(\bar{\gamma},\bar{\eta})(\bar{\tau}_n - \bar{\tau}_n^{crit}(\bar{\gamma},\bar{\eta})), \tag{22}$$

with $A(\bar{\gamma},\bar{\eta})$ the slope of the lines as in Fig. 4.

The averaged contact forces (22) are dependent on the delay $\bar{\tau}_n$ and thus depend on the slowly varying torsional dynamics. Since the bit-rock interaction law provides a coupling between the axial and torsional forces, this will have an impact on the torsional dynamics.

IV. Torsional dynamics

In the analysis of the torsional dynamics, the parameters related to the axial dynamics can be approximated by their averaged values. More specifically, the averaged value over one axial limit cycle will be used, where the limit cycle depends on the instantaneous value of the slowly varying delay $\bar{\tau}_n$. This leads to the approximations

$$g(\dot{u}(\tau)) \approx \langle\bar{g}\rangle_a, \tag{23}$$

$$-u(\tau) + u(\tau-\tau_n) \approx \bar{v}_0\langle -\bar{u}(\bar{\tau}) + \bar{u}(\bar{\tau}-\bar{\tau}_n)\rangle_a = 0, \tag{24}$$

where it is noted that the averaged value over one axial limit cycle is independent of scaling of the time axis. Then, substitution of (23) and (24) in (12) yields

$$\begin{aligned}\ddot{\varphi}(\tau) + (\varphi(\tau) - \theta(\tau)) = &-nv_0(\tau_n - \tau_{n0}) \\ &+ n\beta v_0 A(\bar{\gamma},\bar{\eta})(\tau_n - \tau_n^{crit}(\bar{\gamma},\bar{\eta})),\end{aligned} \tag{25}$$

where (22) and the relation $v_0\tau_n = \bar{v}_0\bar{\tau}_n$ is used. In addition, it is recalled that the delay is (implicitly) given by (14).

It is noted that (25) is only valid when the bit experiences axial stick-slip vibrations, i.e. for $\tau_n > \tau_n^{crit}$. Even though the delay τ_n varies continuously, possibly even stabilizing the axial dynamics, the approximation (25) is valid around the torsional equilibrium point when the nominal delay satisfies $\tau_{n0} = \frac{2\pi}{\omega_0} > \tau_n^{crit}$. Hence, the averaged torsional dynamics (25) can be used to assess stability of the torsional equilibrium point and predict the *onset* of torsional vibrations.

To facilitate stability analysis of the averaged torsional dynamics (25), an explicit expression for the delay τ_n is obtained by using the first-order Taylor approximation $\varphi(\tau - \tau_n) \approx \varphi(\tau) - \dot{\varphi}(\tau)\tau_n$. It is noted that the delay is of $\mathcal{O}(0.1)$, whereas the characteristic time of the torsional dynamics is 2π, which motivates this approach. Then, (14) gives

$$\tau_n \approx \frac{2\pi}{n(\omega_0 + \dot{\varphi}(\tau))}, \tag{26}$$

such that substitution of (26) in (25) yields an autonomous nonlinear approximate of the torsional dynamics. Local stability properties can be determined by the linearization of (26) around $\dot{\varphi} = 0$, which, in combination with (25), yields

$$\ddot{\varphi}(\tau) + (\varphi(\tau) - \theta(\tau)) = nv_0\beta A(\tau_{n0} - \tau_n^{crit}) - nv_0(\beta A - 1)\frac{2\pi}{n\omega_0^2}\dot{\varphi}(\tau). \quad (27)$$

In practice, drag bits are commonly characterized by $\beta < 1$. Furthermore, $A(\bar{\gamma}, \bar{\eta}) < 1$ for realistic parameter values (see e.g. the slopes in Fig. 4), such that $\beta A - 1 < 0$. Hence, the averaged axial dynamics yield a velocity-weakening effect in the bit-rock interaction torque acting on the bit. This leads to unstable torsional dynamics, as can be concluded by the computation of the poles of the linear system (13), (27).

V. Control of the torsional dynamics

In order to (locally) stabilize the torsional dynamics, a controller is designed. Herein, contrary to stability analysis in Section IV, the representation (13-14), (25) will be used for the averaged torsional dynamics, which does not require an approximation of the delay τ_n. By using (14), (25) yields

$$\ddot{\varphi}(\tau) + (\varphi(\tau) - \theta(\tau)) = nv_0\beta A(\tau_{n0} - \tau_n^{crit}) - nv_0\omega_0^{-1}(\beta A - 1)(\varphi(\tau) - \varphi(\tau - \tau_n)). \quad (28)$$

Now, the dynamics (13), (28) is written in state-space form as

$$\dot{x}(\tau) = A_0 x(\tau) + A_1 x(\tau - \tau_n) + B\mathcal{R}_{fb}. \quad (29)$$

with $x^{\mathrm{T}} = \left[\, \varphi \;\; \dot{\varphi} \;\; (\varphi - \theta - nv_0\beta A(\tau_{n0} - \tau_n^{crit})) \;\; \dot{\theta} \,\right]$ and

$$A_0 = \begin{bmatrix} 0 & 1 & 0 & 0 \\ -c & 0 & -1 & 0 \\ 0 & 1 & 0 & -1 \\ 0 & 0 & \rho^{-1} & 0 \end{bmatrix}, \; A_1 = \begin{bmatrix} 0 & 0 & 0 & 0 \\ c & 0 & 0 & 0 \\ 0 & 0 & 0 & 0 \\ 0 & 0 & 0 & 0 \end{bmatrix}, \; B = \begin{bmatrix} 0 \\ 0 \\ 0 \\ \rho^{-1} \end{bmatrix} \quad (30)$$

with $c = nv_0\omega_0^{-1}(\beta A - 1)$. Here, the input torque is split into a feedforward part $\mathcal{R}_{ff}$ and a feedback part $\mathcal{R}_{fb}$ as

$$\mathcal{R} - \mathcal{R}_0 = \mathcal{R}_{ff} + \mathcal{R}_{fb}, \; \mathcal{R}_{ff} = -nv_0\beta A(\tau_{n0} - \tau_n^{crit}). \quad (31)$$

The third state component in the state x represents the deviation from the nominal deflection of the drill string. Herein, the constant term $nv_0\beta A(\tau_{n0} - \tau_n^{crit})$ amounts to the fact that the average torque-on-bit is decreased due to the presence of axial vibrations, reducing the nominal drill string deflection and creating a new equilibrium (i.e. $x = 0$ if $\mathcal{R}_{fb}$ is designed such that $\mathcal{R}_{fb} = 0$ if $x = 0$). For the nominal angular velocity to remain unchanged under the decreased averaged torque-on-bit, the nominal torque on the rotary table has to be decreased as well. This is ensured by the inclusion of the feed-forward torque $\mathcal{R}_{ff}$ in (31). Finally, it is recalled that the delay τ_n is dependent on the state x through (14).

The following result is exploited for control design:

Lemma 1 ([15]): A system $\dot{x}(\tau) = \bar{A}_0 x(\tau) + A_1 x(\tau - \tau_n)$, where the delay τ_n, $0 < \tau_n \leq \tau_n^{max}$, may depend on the history of the state $x(\tau - s)$, $0 \leq s \leq \tau_n^{max}$, is asymptotically stable if there exists a scalar $\alpha > 0$ a matrix $P = P^{\mathrm{T}}$ such that

$$\begin{bmatrix} P\bar{A}_0 + \bar{A}_0^{\mathrm{T}}P + \alpha P & PA_1 \\ A_1^{\mathrm{T}}P & -\alpha P \end{bmatrix} \prec 0, \quad (32)$$

where $X \prec 0$ denotes a negative definite (symmetric) matrix.

This result follows from the Razumikhin theorem and is independent of the maximum delay τ_n^{max}. Lemma 1 can be used for the design of a state feedback controller as follows:

Theorem 1: Consider a system of the form (29), (14). Let there exist matrices $S = S^{\mathrm{T}}$, X and a scalar $\alpha > 0$ such that

$$\begin{bmatrix} A_0 S + SA_0^{\mathrm{T}} + BX + X^{\mathrm{T}}B^{\mathrm{T}} + \alpha S & A_1 S \\ SA_1^{\mathrm{T}} & -\alpha S \end{bmatrix} \prec 0 \quad (33)$$

holds. Then, there exists a compact domain $\mathcal{S} \ni 0$ such that the feedback controller $\mathcal{R}_{fb} = Fx(\tau)$ with $F = XS^{-1}$ renders the equilibrium $x = 0$ of the closed-loop dynamics (29), (14) with $\mathcal{R}_{fb} = Fx(\tau)$ asymptotically stable for all initial conditions satisfying $x(0 + s) \in \mathcal{S}$ $\forall s \in [-\tau_n, 0]$.

Proof: To prove the statement, it is noted that substitution of the control law $\mathcal{R}_{fb} = Fx(\tau)$ in (29) leads to a system as in Lemma 1 with $\bar{A}_0 = A_0 + BF$. Then, a congruence transformation $\mathrm{diag}\{S, S\}$ with $S = P^{-1}$ on (32) and the introduction of the matrix $X = FS$ shows that (33) is equivalent to the condition (32) in Lemma 1.

However, to exploit Lemma 1, it remains to be shown that the delay τ_n as given by (14) is bounded (i.e. the maximum delay τ_n^{max} in Lemma 1 exists). Namely, since the delay is state-dependent, boundedness of τ_n is not automatically guaranteed. Thereto, the following steps are taken.

First, under the assumption that τ_n is indeed bounded, the fulfilment of the condition (33) implies that the domains $\mathcal{D}_c = \{x \in \mathbb{R}^4 \mid V(x) \leq c\}$ with the Razumikhin function $V(x) = x^{\mathrm{T}}Px$ are positively invariant, for all $c \geq 0$. Stated differently, if $x(\tau + s) \in \mathcal{D}_c$ $\forall s \in [-\tau_n^{max}, 0]$, then $x(\tau)$ is in $\mathcal{D}_c$ for all future time. Secondly, it is noted that the condition $\dot{\varphi}(\tau) > -v_0$ is sufficient for the delay τ_n to be bounded (see (14)). Namely, the delay can only grow unbounded when the bit sticks axially (i.e. $\dot{\varphi}(\tau) = -v_0$). Since the equilibrium point $x = 0$ is separated from the line $\dot{\varphi} = -v_0$, there exists $\tilde{c}^*$ such that for all $\tilde{c} \in [0, \tilde{c}^*]$ the condition $x(\tau + s) \in \mathcal{D}_{\tilde{c}}$ $\forall s \in [-\tau_n, 0]$ and $\forall \tau \geq 0$ implies that the delay τ_n is bounded. Hence, when the initial condition for the closed-loop dynamics (29), (14) with $\mathcal{R}_{fb} = Fx(\tau)$ is chosen such that $x(0 + s) \in \mathcal{D}_{\tilde{c}}$ $\forall s \in [-\tau_n, 0]$, the fact that the set $\mathcal{D}_{\tilde{c}}$ is positively invariant implies that the delay τ_n remains bounded, such that τ_n^{max} in Lemma 1 exists, completing the proof with $\mathcal{S} = \mathcal{D}_{\tilde{c}}$. ■

It is noted that the matrix condition (33) is a linear matrix inequality in the matrices S and X, when α is fixed. Since efficient methods are available for solving linear matrix inequalities, Theorem 1 directly provides a tool for controller synthesis, where a line search over α can be employed.

Remark 1: Even though Theorem 1 facilitates control design such that asymptotic stability of $x = 0$ in (29) (i.e. (13), (28)) with (14) and (31) can be guaranteed, application of this controller to the full coupled dynamics (11-14) does not necessarily lead to the stabilization of the torsional dynamics. Clearly, in this control design, the axial dynamics is only taken into account using averaging, such that Theorem 1 can not be used to prove stability of the controlled full dynamics. In addition, to facilitate averaging, the separation

TABLE I

Parameter values for the dynamics (11-14).

v_0	2	β	0.276	
ω_0	4	γ	0.973	$(\bar{\gamma} = 0.05)$
λ	0.9	η^2	37.8	$(\bar{\eta}^2 = 0.1)$
$n\psi$	$6 \cdot 63.1$	ρ	10	

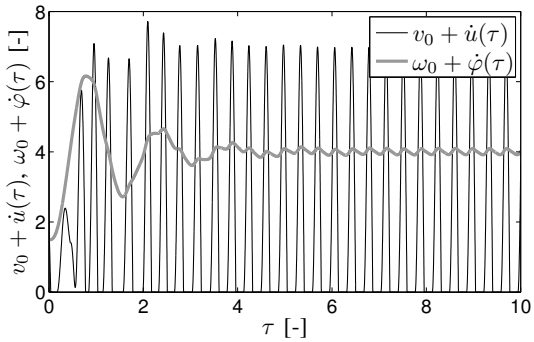

Fig. 5. closed-loop dynamics with the parameters in Table I: bit axial and angular velocity $\dot{u}(\tau)$ and $\dot{\varphi}(\tau)$.

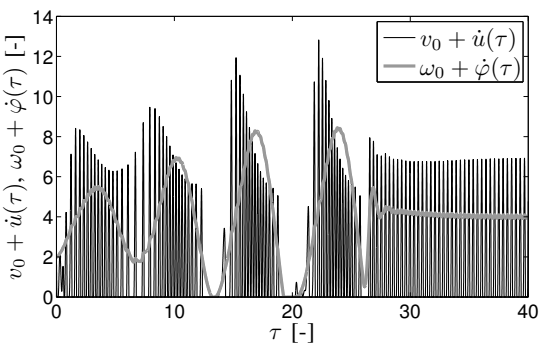

Fig. 6. closed-loop dynamics with the parameters in Table I: bit axial and angular velocity $\dot{u}(\tau)$ and $\dot{\varphi}(\tau)$. The controller is switched on at $\tau = 25$.

of time scales between the (fast) axial dynamics and (slow) torsional dynamics was exploited. Hence, the controlled torsional dynamics can only be expected to be stable when this separation is maintained.

Nonetheless, Theorem 1 is applied to obtain a controller with gain $F = 10^3 \cdot \begin{bmatrix} -3.4485 & -1.5747 & 0.4818 & -0.0890 \end{bmatrix}$, hereby using the parameter values in Table I. It is noted that this controller is not unique, but is guaranteed to stabilize the averaged torsional dynamics (13-14), (28). This state feedback controller is implemented on the full dynamics (11-14). A simulation of this controlled system is depicted in Fig. 5, where $\dot{\varphi}(0) = -2.5$, $\varphi(\tau) = 0$ for all $\tau \leq 0$ and $\theta(0) = \dot{\theta}(0) = 0$. It is clear that the controller indeed stabilizes the torsional dynamics, even though the axial dynamics continues to exhibit stick-slip limit cycles. Additionally, the controller reduces the time scale of the torsional dynamics, such that the approximation (28) no longer holds. Nonetheless, the controller gives a good performance.

Finally, a simulation is performed in which the controller is switched on when the torsional dynamics exhibits a torsional stick-slip limit cycle. It is recalled that torsional stick is not included in the model (11-14), but it is included for this simulation using the description in [8]. The result is depicted in Fig. 6, from which it can be concluded that the controller suppresses the torsional stick-slip limit cycle.

VI. Conclusions

In this work, the mechanisms leading to torsional vibrations in drilling systems are analyzed. Herein, the approach as in [5] and [7] is followed, where the model is extended with the essential aspects of axial flexibility of the drill string, axial friction along the bottom hole assembly and the torsional dynamics of the rotary table. Analysis of this model shows that the (fast) axial dynamics exhibits a stick-slip limit cycle. This generates an apparent velocity-weakening effect in the torque-on-bit, leading to torsional vibrations. In addition, this analysis facilitates the design of a controller aiming to suppress torsional vibrations.

Besides this control design targeting the torsional dynamics directly, the analysis presented in this work may also serve as a basis for the design of active control strategies targeting the axial dynamics. Namely, since the axial dynamics forms the driving force behind the torsional vibrations, stabilization of the torsional dynamics may prevent torsional vibrations as well. Future work will focus on this topic.

References

[1] J. F. Brett, "The genesis of torsional drillstring vibrations," *SPE Drilling Engineering*, vol. 7, no. 3, pp. 168–174, 1992.

[2] N. Challamel, "Rock destruction effect on the stability of a drilling structure," *Journal of Sound and Vibration*, vol. 233, no. 2, pp. 235–254, 2000.

[3] R. W. Tucker and C. Wang, "An integrated model for drill-string dynamics," *Journal of Sound and Vibration*, vol. 224, no. 1, pp. 123–165, 1999.

[4] Y. Nishimatsu, "The mechanics of rock cutting," *International Journal of Rock Mechanics & Mining Sciences*, vol. 9, pp. 261–270, 1972.

[5] T. Richard, C. Germay, and E. Detournay, "A simplified model to explore the root cause of stick-slip vibrations in drilling systems with drag bits," *Journal of Sound and Vibration*, vol. 305, pp. 432–456, 2007.

[6] E. Detournay and P. Defourny, "A phenomenological model for the drilling action of drag bits," *International Journal of Rock Mechanics and Mining Science & Geomechanics Abstracts*, vol. 29, pp. 13–23, 1992.

[7] C. Germay, N. van de Wouw, H. Nijmeijer, and R. Sepulchre, "Nonlinear drillstring dynamics analysis," *SIAM Journal on Applied Dynamical Systems*, vol. 8, no. 2, pp. 527–553, 2009.

[8] B. Besselink, N. van de Wouw, and H. Nijmeijer, "A semi-analytical study of stick-slip oscillations in drilling systems," *Journal of Computational and Nonlinear Dynamics*, vol. 6, no. 2, p. 021006, 2011.

[9] J. C. A. de Bruin, A. Doris, N. van de Wouw, W. P. M. H. Heemels, and H. Nijmeijer, "Control of mechanical motion systems with non-collocation of actuation and friction: A Popov criterion approach for input-to-state stability and set-valued nonlinearities," *Automatica*, vol. 45, no. 2, pp. 405–415, 2009.

[10] A. P. Christoforou and A. S. Yigit, "Fully coupled vibrations of actively controlled drillstrings," *Journal of Sound and Vibration*, vol. 267, no. 5, pp. 1029–1045, 2003.

[11] J. D. Jansen and L. van den Steen, "Active damping of self-excited torsional vibrations in oil well drillstrings," *Journal of Sound and Vibration*, vol. 179, no. 4, pp. 647–668, 1995.

[12] E. M. Navarro-López and R. Suarez, "Practical approach to modelling and controlling stick-slip oscillations in oilwell drillstrings," in *Proceedings of the IEEE International Conference on Control Applications, Taipei, Taiwan*, vol. 2, 2004, pp. 1454–1460.

[13] A. F. Filippov, *Differential equations with discontinuous righthand sides*. Kluwer Academic Publishers, Dordrecht, 1988.

[14] W. Michiels and S.-I. Niculescu, *Stability and stabilization of time-delay systems: an eigenvalue-based approach*. SIAM, Philadelphia, 2007.

[15] K. Gu, V. L. Kharitonov, and J. Chen, *Stability of time-delay systems*. Birkhäuser, Boston, 2003.